ACS Energy LETTERS

http://pubs.acs.org/journal/aelccp

VIEWPOINT

On Lifetime and Cost of Redox-Active Organics for Aqueous Flow Batteries

Cite This: *ACS Energy Lett.* 2020, 5, 879−884

Read Online

ACCESS | Metrics & More | Article Recommendations | Supporting Information

Stationary electric energy storage is anticipated to play an increasingly important role in the efficient, reliable, and sustainable delivery of electricity, especially with increasing deployment of low cost intermittent renewable energy sources. Redox flow batteries (RFBs) are a promising electrochemical technology whose decoupling of power and energy scaling, long operational lifetimes, and safety are particularly appealing for energy storage with long discharge duration. The recent emergence of aqueous organic redox flow batteries (AORFBs) offers intriguing new pathways to inexpensive energy storage through the use of charge storage materials that are composed of earth-abundant elements and have the potential for cost-effective mass production, and whose electrochemical and physicochemical properties can be tuned through molecular functionalization.[1−3] Further, redox-active organics possess several secondary benefits, including compatibility across a wide pH range, rapid redox kinetics with multielectron transfer, and low permeability through polymeric membranes. Over the past decade, many organic and organometallic molecular families have been proposed and pursued, including but not limited to quinones,[1,4−10] viologens,[11−13] nitroxide radicals,[11,12,14−18] aza-aromatics,[19−24] and iron coordination complexes.[13,25] In addition, several start-up companies have emerged seeking to translate these scientific advances into cost-competitive energy solutions, such as Kemiwatt (France), Green Energy Storage (Italy), XL Batteries (United States), and JenaBatteries and CMBlu (Germany).

Despite this progress, molecular lifetime remains a significant challenge for practical deployment for AORFBs.[13,26] Initial durability experiments tend to involve repetitive galvanostatic charge−discharge cycles, typically in a bulk electrolysis cell, at low concentrations and/or small electrolyte volumes to reduce the materials- and time-intensity of experiments. Thus, early claims of long cycle life are often based on a large number of cycles without significant decay performed over a short period of time. With recent advances in the field, it has become evident that all reasonably long-lived molecular redox couples (here, defined as having a half-life greater than a day) of which we are aware, when sufficiently thorough experiments to distinguish between cycle- and calendar-denominated fade have been performed, have shown decay to be time-dependent and a function of temperature, state of charge (SOC), molecular concentration, pH, and electrostatic potential.[7,8,13,26] Generally, albeit with some exceptions,[7] the molecule is more suspectible to decay in its "energized" state (i.e., the oxidized state for the posolyte or the reduced state for the negolyte).

The continued development of AORFBs requires the adoption of more rigorous testing protocols to accurately assess molecular lifetimes, to elucidate the subtle failure modes of increasingly robust molecules, and to maintain the iterative design−test−improve cycle. Moreover, as the cost-effectiveness of AORFBs is dependent on the chemical costs and fade rates of finite-lifetime organics, as opposed to the current state-of-the-art vanadium, we aim to help guide and accelerate research efforts by articulating a feasible design space for the community to target. In this Viewpoint, we first outline experimental protocols that we urge those active in the field to adopt to better quantify capacity fade. Subsequently, we extend an existing bottom-up capital cost model to estimate AORFB system cost as a function of molecular lifetime, chemical costs, and the interest rate for discounting. While we limit our focus to aqueous-soluble organics, we anticipate the following approaches are applicable to all molecular redox-active materials for which lifetime is uncertain.

Capacity Fade Rate Protocol. The procedures summarized below are recommended because they improve the accuracy and simplify the interpretation of capacity fade rates due to molecular decomposition. It is encumbent upon the researcher to determine how closely to follow these procedures, based on prior evidence, the value of time in a study, or whether certain analyses should be expanded upon to address chemistry-dependent phenomena. We note that these procedures are representative and intended as guidance to the greater community. There is room and need for continued innovation and advancement in this discipline.

Cell Configuration. A volumetrically unbalanced, compositionally symmetric flow cell configuration,[26,27] in which the same compound fills both reservoirs at an intermediate state of charge (SOC), is recommended for characterizing capacity fade rates (Figure 1a). The symmetric flow cell technique offers a controlled electrolyte environment by removing the need for a counter electrode of dissimilar material, suppressing

Received: January 19, 2020
Accepted: February 7, 2020

https://dx.doi.org/10.1021/acsenergylett.0c00140
ACS Energy Lett. 2020, 5, 879−884

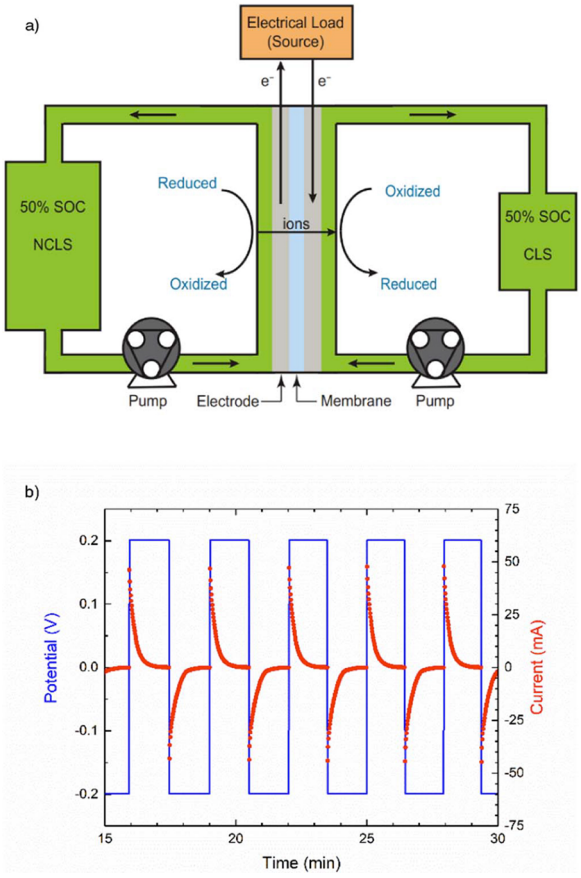

Figure 1. (a) Schematic of volumetrically unbalanced compositionally symmetric cell, with identical electrolytes at identical concentrations at 50% SOC in reservoirs of different volumes. Active species crossover is suppressed, and measured capacity fade may be attributed to the state of the capacity limiting side (CLS). (b) Potentiostatic cycling with polarity switching occurring when the current density drops below 1 mA/cm^2. From ref 26. Copyright 2018.

the loss of capacity through active species crossover. Note, however, that if the oxidized and reduced forms of a species have different membrane permeabilities and the SOC history of the capacity-limiting side is not managed well, then the possibility of net crossover exists even in a symmetric cell. Symmetric compositions also effectively eliminate the possibility of side-product species crossing over from the counter electrode chamber and contaminating the working electrode. The flowing electrolyte improves mass transfer, enabling cycling of concentrated solutions and investigatation of active material stability on high surface area porous electrodes of relevance to practical flow battery applications. Care should be taken when selecting wetted components, and *ex situ* compatibility studies are recommended prior to experimentation. The charge capacity of the electrolyte of interest should first be evaluated with *in situ* or *ex situ* bulk electrolysis, with discussion given to any significant discrepancy from theoretical capacity. The volumes filling the reservoirs should differ so that one side is the capacity-limiting side (CLS) during both oxidation and reduction. The noncapacity-limiting side (NCLS) should have active species in significant excess so that it remains noncapacity-limiting in both oxidation and reduction, even if undesirable side reactions act to drive the cell away from perfect electrolyte balance. If the active species of interest is confined to the CLS and the crossover rates of the active and contaminant species through the membrane are sufficiently low, this methodology can be applied to full cells as well. As a working hypothesis, it is reasonable to assume that the decomposition rates of the individual active species will not change and that the major effect of switching to full-cell configurations would be the additive effect of crossover. However, this hypothesis may be challenged by various effects including differences in the potential gradients within the cell and chemistry-specific interactions between constituent components.

Cycling Methodology. A potentiostatic hold at the end of a charging step and of a subsequent discharging step is essential for accurate capacity measurements. This can be implemented through purely potentiostatic cycling, as in Figure 1b, with the voltage held until the current density drops to very near an empirically determined background value, typically of order 1 mA/cm^2. Galvanostatic cycling, the more common approach to charge−discharge cycling, is vulnerable to artifacts that evolve over time during cell operation and can obscure low capacity fade rates, as shown in Figure 2. While both

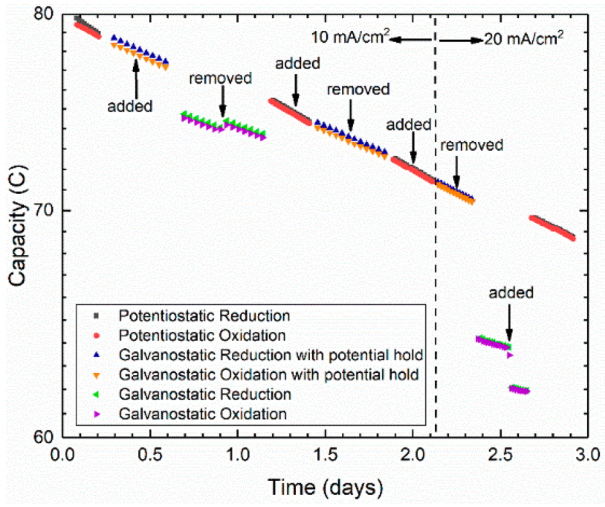

Figure 2. Semilog plot of volumetrically unbalanced compositionally symmetric cell cycling of 2,6-dihydroxyanthraquinone (DHAQ), showing changes in apparent capacity with adjustments to overall cell resistance and current density for purely galvanostatic cycling and the absence of such artifacts under potentiostatic cycling and in galvanostatic cycling with potential holds at the end of each half-cycle. In the latter two cases, cycling was performed by imposing voltage holds at ±200 mV and switched when current density dropped to 1 mA/cm^2. Galvanostatic conditions were started at 10 mA/cm^2 and increased to 20 mA/cm^2 after 2.13 days. Vertical arrows indicate times at which a resistor (130 mΩ, equivalent to a 25% increase in ohmic resistance) was added and removed in series with the cell. The jumps in apparent capacity demonstrate the dependence of apparent cycling capacity on cell resistance when strictly galvanostatic conditions are used. From ref 26. Copyright 2018.

techniques require judicious selection of voltage limits, often established through a combination of voltammetric and mass transport analysis, with constant current operation drifts in the internal resistance of the cell, e.g. from diurnal temperature swings, from aging of the wetted components, and even from pulsatile flow at low SOC, can appear as apparent capacity fade. Alternatively, galvanostatic cycling with a potential hold

https://dx.doi.org/10.1021/acsenergylett.0c00140
ACS Energy Lett. 2020, 5, 879−884

at the end of each half-cycle is an effective means of eliminating these artifacts and isolating the true capacity fade rate (Figure 2). If, for whatever reason, it is necessary to evaluate the capacity fade rate during purely galvanostatic cycling, it is recommend that one in every *n*th cycle is followed by a potential hold in the charging and discharging half-cycles and that the discharge capacities from only these cycles be used to assess capacity fade rate. The inclusion of pauses at various SOCs can enable assessment of SOC-dependent temporal fade rates upon the resumption of cycling, as illustrated in Figure 3.

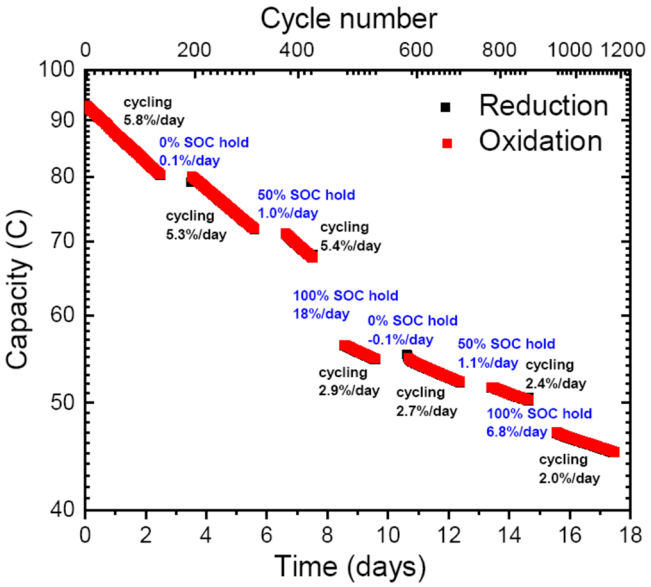

Figure 3. Semilog plot of volumetrically unbalanced compositionally symmetric cell cycling of 50% SOC 0.1 M DHAQ in 1 M KOH with cycling pauses in different states of charge. Instantaneous decay rates derived from slopes of each cycling segment are denoted in black text. Decay rates during holding periods at various SOCs are denoted in blue text. Every 20th cycle is denoted by a tick mark along the top axis. Adapted from ref 26. Copyright 2018.

Systematic variations in cycle period can, in principle, uniquely disaggregate cycle-dominated fade rates from time-dominated fade rates; however, as Figure 3 shows, the instantaneous fade rate may also depend on the remaining capacity.

Data Interpretation. Only after the capacity has faded to a value measurably below the capacity measured originally in a bulk electrolysis experiment can one begin to interpret capacity fade rate measurements quantitatively. Before that, it is unclear whether the apparent capacity is being maintained by recruiting species that, for whatever reason, were not accessed during the first few cycles. For example, the presence of residual dissolved O_2 in the electrolyte at the start of cycling experiments may disturb initial cycles by chemically oxidizing a reduced negative electrolyte.

If it is suspected that the NCLS may have become capacity-limiting during the cycling experiment, at the end of cycling the NCLS should be replaced with fresh electrolyte and a few additional full charge−discharge cycles imposed to confirm the final capacity of the CLS. If a cycling regimen involves a restricted SOC swing, its capacity fade rate should be evaluated by comparing full charge−discharge cycles immediately before and after the restricted SOC regimen: otherwise, it is unclear whether the apparent capacity is being maintained by recruiting species that were not accessed during the restricted SOC swing regimen.

Should capacity fade rates be too low to measure with confidence, it may be helpful to accelerate reactions by increasing temperature, either of electrolytes in isolation or within an operating cell. For example, it is straightforward, though tedious, to hold both the oxidized and reduced forms (the latter may need to be very well protected from air, as described in the Supporting Information in ref 8) at elevated temperature for multiple days and perform extensive chemical analyses (e.g., mass spectrometry, NMR, and cyclic voltammetry). However, caution should be taken as the dominant mechanism may be temperature-dependent; additionally, redox-active and inactive decomposition products must be distinguished. Furthermore, active species lifetimes may be different in isolation than in contact with wetted materials in an operating cell.

Data Reporting. It is recommended that both capacity fade rate per day and per cycle be reported. If, as is typical, a certain fractional capacity loss is observed but not uniquely decomposed into cycle- and time-denominated rates, then the capacity fade rate can be reported as "*X*% per day or *Y*% per cycle". Capacity fade rate rather than capacity retention rate should be reported because the arithmetic for converting between hourly, daily, and annual fade rates is simpler than that for converting between the corresponding capacity retention rates. It is important to report sufficient information regarding the experimental methods, including electrolyte volumes, to enable a knowledgeable colleague to reproduce the experimental results.

Cost−Lifetime Trade-off. Under certain scenarios, molecular lifetime does not have to be infinite for an organic chemistry to be potentially lower in cost than the incumbent vanadium chemistry. Indeed, the up-front capital cost savings of using an inexpensive organic instead of vanadium can be compared with the present value of a series of future replacement costs, recognizing the time-value of money. The trade-off is quantified by a replacement cost ratio, defined as the annual replacement cost divided by the up-front capital cost savings.[2] The break-even value of the replacement cost ratio depends on the interest rate for discounting and the project lifetime, as shown in Figure 4. When the actual value of the replacement cost ratio is less than this break-even value, organics are potentially lower-cost than vanadium. For example, if the organic is 40% of the cost of vanadium per kilowatt-hour but loses 9% per year, then the replacement cost ratio is (0.09)(0.4)/(1.0 − 0.4) = 0.06 and a 20-year project breaks even at an interest rate of 1.8%, with higher interest rates favoring the organic. If one anticipates an infinite-year project for vanadium, enabled by periodic electrolyte maintenance, then under the same assumptions as before, break even would occur at an interest rate of 6.0%. This simple comparison assumes zero reconditioning cost when organic or vanadium replacements occur, but the model can be generalized by adding reconditioning cost.

Design Space for Electrolytes of Finite Lifetime. The effects of finite electrolyte lifetime and necessary replacements can be integrated into existing capital cost models to account for the present value of a series of future chemical replacement costs and to outline the allowable ranges of chemical costs, fade rates, and discounting rates and their dependence on other relevant cost-constraining parameters.[28,29] For brevity, the mathematical manipulations, simplifying assumptions, and

https://dx.doi.org/10.1021/acsenergylett.0c00140
ACS Energy Lett. 2020, 5, 879−884

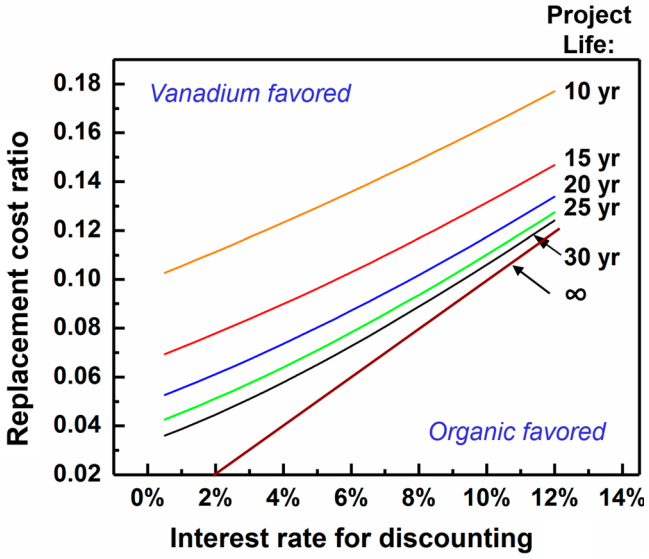

Figure 4. Break-even value of replacement cost ratio vs interest rate for discounting, assuming project lifetimes as indicated. Adapted from ref 2. Copyright 2018.

baseline model inputs are detailed in the Supporting Information. Here, we illustrate the impact of periodic electrolyte replacement on the economic viability of AORFBs as a function of capacity fade rate, discount rate, and discharge duration and properties of the redox chemistry (e.g., cell potential, chemical costs, and cell resistance) (Figure 5). As shown in Figure 5a, AORFBs with high cell voltages and low total active costs have reduced up-front capital costs, especially at longer discharge durations (10−100 h) where the system cost is dominated by the electrolyte materials.[30] For comparison, the vanadium RFB capital costs, assuming no electrolyte maintenance or replacement over the project lifetime, are shown as a function of vanadium pentoxide precursor prices (average ± standard deviation) based on publicly available data from the past three years.[31] For reference, capital costs of vanadium RFBs are frequently cited between 300 and 500 $/kWh, and our calculated values fall within this range at comparable storage durations (1−10 h).[32−34] The variability in vanadium price, dictated by other industries (e.g., steel manufacturing), offers a window for finite-lifetime organics provided the redox chemistries have suitable combinations of high cell voltages and low electrolyte costs. The latter may be realized through a balance of inexpensive chemicals, low fade rates, and favorable interest rates for discounting (Figure 5b). Visualizing the dependence and sensitivity of capital cost to total active cost as a function of cell potential, cell resistance, and duration also provides

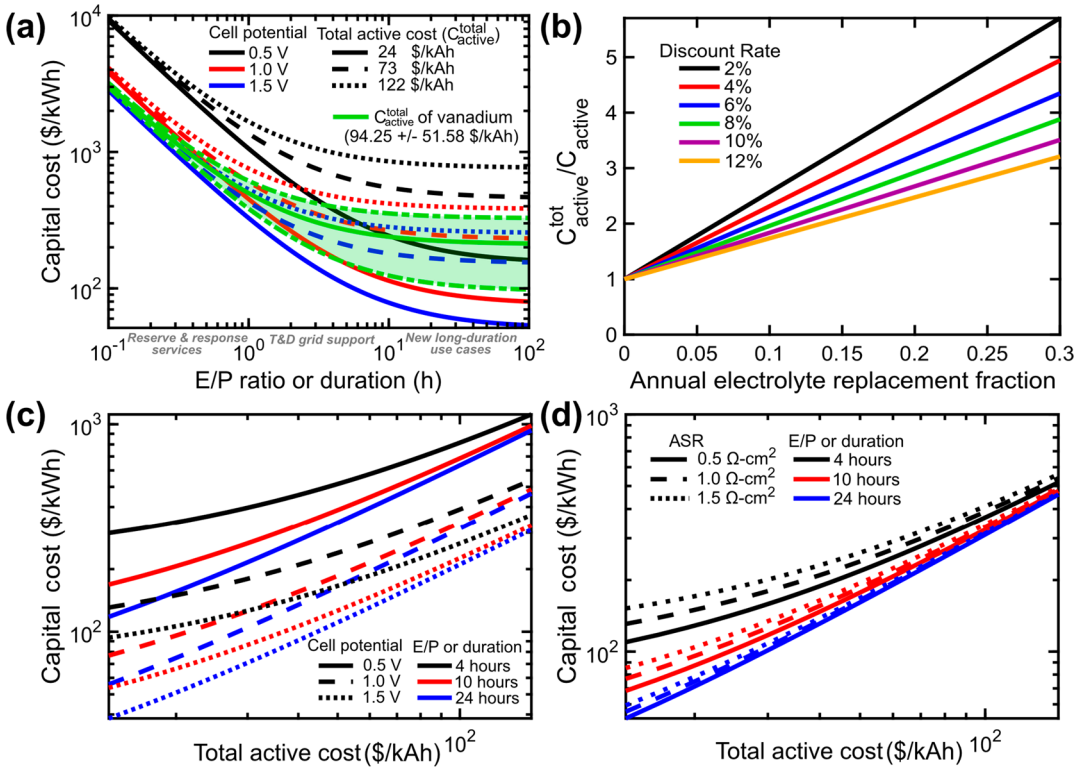

Figure 5. Capital cost modeling of generic RFBs incorporating the net present value of the finite-life electrolytes. (a) Capital cost decreases with longer discharge duration, higher power reactors, and inexpensive electrolytes. At long durations (10−100 h) the system costs begin to asymptotically approach that cost of the electrolyte in the reservoirs. The cost of vanadium RFBs for a range of recent historical vanadium prices is provided as a comparison. (b) The total active costs, which is directly proportional to the electrolyte cost, is a function of the chemical cost, the fade rate, and the discount rate. Capital cost vs total active cost for various discharge durations and (c) cell potentials; (d) area-specific resistances (ASRs). At low total active costs, the capital cost of the cell shows greater sensivity to cell potential, discharge duration, and cell resistance. At high total active costs, the electrolyte dominates the capital cost and, with an exception of cell voltage which impacts both power and energy costs, there is little differentiation between the other parameters. For the data shown in panels a−c, a cell ASR of 1.0 Ω·cm² is assumed, and for panel d, a cell voltage of 1.0 V is assumed. Further details on model inputs, formulation, and data visualization can be found in the Supporting Information.

https://dx.doi.org/10.1021/acsenergylett.0c00140
ACS Energy Lett. 2020, 5, 879−884

insight into the relative importance of reactor performance and cost in defining cost-effective applications spaces (Figure 5c,d).

Summary. The cost of electrolyte materials for a RFB is a dominant factor for systems with high E/P ratios. For aqueous systems, in which the solvent and salt are generally inexpensive, the cost of the active materials is of greatest concern. Organic active materials, made of earth-abundant elements, can be, but are not necessarily, low-cost after synthesis. However, their finite lifetimes raise their costs by adding a periodic replacement cost that complicates techno-economic assessments. We have described the best methods available to us at this time on how to assess the lifetime of organic active materials. We have shown how to factor the lifetime into an estimate of the system cost per kilowatt-hour of energy storage capacity. The total active cost is directly proportional to the capital cost per kilowatt-hour of the active materials and is a function of the annual replacement ratio and the interest rate for discounting future expenses to the present. The cost of incumbent vanadium RFBs serves as a convenient foil for comparison. These results begin to define a design space for cost-competitive AORFBs that necessitates materials of sufficiently disparate redox potentials that are stable and economical. Of the numerous and expanding variety of organic redox couples reported in the literature,[35] a few redox chemistries with high cell potential (≥1 V) and stability (ca. 5% per annum or less)[8] can be identified, although, to the authors' knowledge, none has been tested for durations approaching a year. In parallel, recent initial process economic assessments by Yang et al. and Dieterich et al. have shown potential pathways to low-cost materials (ca. $35/kAh per side, or less),[2,3] but those materials are often associated with higher fade rates. As the field progresses, further work is needed to articulate the scientific and economic trade-offs between materials cost, stability, and ease of recovery. To this last point, recent work has demonstrated the potential for *in situ* regeneration,[36] which may eventually serve as a capacity recovery mechanism similar to electrolyte rebalancing in vanadium RFBs, further improving the prospects of potentially inexpensive materials with moderate fade rates. Ultimately, the authors hope that this Viewpoint provides guidance to the research community and inspires new research directions that further advance the science and engineering of AORFBs.

Fikile R. Brushett orcid.org/0000-0002-7361-6637
Michael J. Aziz orcid.org/0000-0001-9657-9456
Kara E. Rodby

■ ASSOCIATED CONTENT

Supporting Information

The Supporting Information is available free of charge at https://pubs.acs.org/doi/10.1021/acsenergylett.0c00140.

Mathematical formulations, model inputs, and simplifying assumptions regarding the techno-economic analyses performed in this work (PDF)

■ AUTHOR INFORMATION

Complete contact information is available at:
https://pubs.acs.org/10.1021/acsenergylett.0c00140

Author Contributions

M.J.A.: conceptualization, methodology, writing—original draft, supervision, funding acquisition; FRB: methodology, writing—original draft, resources, supervision, funding acquisition; KER: methodology, software, investigation, visualization.

Notes

Views expressed in this Viewpoint are those of the authors and not necessarily the views of the ACS.
The authors declare no competing financial interest.

■ ACKNOWLEDGMENTS

Work at Harvard was supported by U.S. DOE award DE-AC05-76RL01830 through PNNL subcontract 428977, by ARPA-E award DE-AR0000767, by Innovation Fund Denmark via the Grand Solutions project "ORBATS" file nr. 7046-00018B, and by the Massachusetts Clean Energy Technology Center. Work at MIT was supported by the Joint Center for Energy Storage Research (JCESR), an Energy Innovation Hub funded by the United States Department of Energy, Office of Science, Basic Energy Sciences (DE-AC02-06CH11357). The authors thank Eric Fell, Martin Jin, Yan Jing, Emily Kerr, Daniel Pollack, Zhijiang Tang, Andrew Wong, and Min Wu (Harvard) as well as Michael Orella (MIT) for helpful comments.

■ REFERENCES

(1) Huskinson, B. T.; Marshak, M. P.; Suh, C.; Er, S.; Gerhardt, M. R.; Galvin, C. J.; Chen, X.; Aspuru-Guzik, A.; Gordon, R. G.; Aziz, M. J. A Metal-Free Organic-Inorganic Aqueous Flow Battery. *Nature* **2014**, *505*, 195.
(2) Yang, Z.; Tong, L.; Tabor, D. P.; Beh, E. S.; Goulet, M. A.; De Porcellinis, D.; Aspuru-Guzik, A.; Gordon, R. G.; Aziz, M. J. Alkaline Benzoquinone Aqueous Flow Battery for Large-Scale Storage of Electrical Energy. *Adv. Energy Mater.* **2018**, *8*, 1702056.
(3) Dieterich, V.; Milshtein, J. D.; Barton, J. L.; Carney, T. J.; Darling, R. M.; Brushett, F. R. Estimating the Cost of Organic Battery Active Materials: A Case Study on Anthraquinone Disulfonic Acid. *Transl. Mater. Res.* **2018**, *5*, 034001.
(4) Yang, B.; Hoober-Burkhardt, L.; Wang, F.; Surya Prakash, G. K.; Narayanan, S. R. An Inexpensive Aqueous Flow Battery for Large-Scale Electrical Energy Storage Based on Water-Soluble Organic Redox Couples. *J. Electrochem. Soc.* **2014**, *161*, A1371.
(5) Lin, K.; Chen, Q.; Gerhardt, M. R.; Tong, L.; Kim, S. B.; Eisenach, L.; Valle, A. W.; Hardee, D.; Gordon, R. G.; Aziz, M. J.; Marshak, M. P. Alkaline Quinone Flow Battery. *Science* **2015**, *349*, 1529.
(6) Hoober-Burkhardt, L.; Krishnamoorthy, S.; Yang, B.; Murali, A.; Nirmalchandar, A.; Prakash, G. K. S.; Narayanan, S. R. A New Michael-Reaction-Resistant Benzoquinone for Aqueous Organic Redox Flow Batteries. *J. Electrochem. Soc.* **2017**, *164*, A600.
(7) Kwabi, D. G.; Lin, K.; Ji, Y.; Kerr, E. F.; Goulet, M.-A.; De Porcellinis, D.; Tabor, D. P.; Pollack, D. A.; Aspuru-Guzik, A.; Gordon, R. G.; Aziz, M. J. Alkaline Quinone Flow Battery with Long Lifetime at pH 12. *Joule* **2018**, *2*, 1907.
(8) Ji, Y.; Goulet, M. A.; Pollack, D. A.; Kwabi, D. G.; Jin, S.; Porcellinis, D.; Kerr, E. F.; Gordon, R. G.; Aziz, M. J. A Phosphonate-Functionalized Quinone Redox Flow Battery at Near-Neutral pH with Record Capacity Retention Rate. *Adv. Energy Mater.* **2019**, *9*, 1900039.
(9) Tong, L.; Goulet, M.-A.; Tabor, D. P.; Kerr, E. F.; De Porcellinis, D.; Fell, E. M.; Aspuru-Guzik, A.; Gordon, R. G.; Aziz, M. J. Molecular Engineering of an Alkaline Naphthoquinone Flow Battery. *ACS Energy Letters* **2019**, *4*, 1880.
(10) Jin, S.; Jing, Y.; Kwabi, D. G.; Ji, Y.; Tong, L.; De Porcellinis, D.; Goulet, M. A.; Pollack, D. A.; Gordon, R. G.; Aziz, M. J. A Water-Miscible Quinone Flow Battery with High Volumetric Capacity and Energy Density. *ACS Energy Letters* **2019**, *4*, 1342.
(11) Liu, T. B.; Wei, X. L.; Nie, Z. M.; Sprenkle, V.; Wang, W. A Total Organic Aqueous Redox Flow Battery Employing a Low Cost and Sustainable Methyl Viologen Anolyte and 4-HO-TEMPO Catholyte. *Adv. Energy Mater.* **2016**, *6*, 1501449.

(12) Janoschka, T.; Martin, N.; Martin, U.; Friebe, C.; Morgenstern, S.; Hiller, H.; Hager, M. D.; Schubert, U. S. An Aqueous, Polymer-Based Redox-Flow Battery Using Non-Corrosive, Safe, and Low-Cost Materials. *Nature* **2015**, *527*, 78.
(13) Beh, E. S.; De Porcellinis, D.; Gracia, R. L.; Xia, K. T.; Gordon, R. G.; Aziz, M. J. A Neutral pH Aqueous Organic-Organometallic Redox Flow Battery with Extremely High Capacity Retention. *ACS Energy Letters* **2017**, *2*, 639.
(14) Janoschka, T.; Martin, N.; Hager, M. D.; Schubert, U. S. An Aqueous Redox-Flow Battery with High Capacity and Power: The TEMPTMA/MV System. *Angew. Chem., Int. Ed.* **2016**, *55*, 14427.
(15) Winsberg, J.; Janoschka, T.; Morgenstern, S.; Hagemann, T.; Muench, S.; Hauffman, G.; Gohy, J. F.; Hager, M. D.; Schubert, U. S. Poly(TEMPO)/Zinc Hybrid-Flow Battery: A Novel, 'Green,' High Voltage, and Safe Energy Storage System. *Adv. Mater.* **2016**, *28*, 2238.
(16) Orita, A.; Verde, M. G.; Sakai, M.; Meng, Y. S. The Impact of pH on Side Reactions for Aqueous Redox Flow Batteries Based on Nitroxyl Radical Compounds. *J. Power Sources* **2016**, *321*, 126.
(17) Hu, B.; Tang, Y.; Luo, J.; Grove, G.; Guo, Y.; Liu, T. L. Improved Radical Stability of Viologen Anolytes in Aqueous Organic Redox Flow Batteries. *Chem. Commun. (Cambridge, U. K.)* **2018**, *54*, 6871.
(18) Liu, Y. H.; Goulet, M. A.; Tong, L. C.; Liu, Y. Z.; Ji, Y. L.; Wu, L.; Gordon, R. G.; Aziz, M. J.; Yang, Z. J.; Xu, T. W. A Long-Lifetime All-Organic Aqueous Flow Battery Utilizing TMAP-TEMPO Radical. *Chem.* **2019**, *5*, 1861.
(19) Milshtein, J. D.; Su, L.; Liou, C.; Badel, A. F.; Brushett, F. R. Voltammetry Study of Quinoxaline in Aqueous Electrolytes. *Electrochim. Acta* **2015**, *180*, 695.
(20) Lin, K.; Gomez-Bombarelli, R.; Beh, E. S.; Tong, L.; Chen, Q.; Valle, A.; Aspuru-Guzik, A.; Aziz, M. J.; Gordon, R. G. A Redox-Flow Battery with an Alloxazine-Based Organic Electrolyte. *Nature Energy* **2016**, *1*, 16102.
(21) Orita, A.; Verde, M. G.; Sakai, M.; Meng, Y. S. A Biomimetic Redox Flow Battery Based on Flavin Mononucleotide. *Nat. Commun.* **2016**, *7*, 13230.
(22) Hollas, A.; Wei, X. L.; Murugesan, V.; Nie, Z. M.; Li, B.; Reed, D.; Liu, J.; Sprenkle, V.; Wang, W. A Biomimetic High-Capacity Phenazine-Based Anolyte for Aqueous Organic Redox Flow Batteries. *Nature Energy* **2018**, *3*, 508.
(23) Huang, J. H.; Yang, Z.; Murugesan, V.; Walter, E.; Hollas, A.; Pan, B. F.; Assary, R. S.; Shkrob, I. A.; Wei, X. L.; Zhang, Z. C. Spatially Constrained Organic Diquat Anolyte for Stable Aqueous Flow Batteries. *ACS Energy Letters* **2018**, *3*, 2533.
(24) Zhang, C.; Niu, Z.; Peng, S.; Ding, Y.; Zhang, L.; Guo, X.; Zhao, Y.; Yu, G. Phenothiazine-Based Organic Catholyte for High-Capacity and Long-Life Aqueous Redox Flow Batteries. *Adv. Mater.* **2019**, *31*, 1901052.
(25) Hu, B.; DeBruler, C.; Rhodes, Z.; Liu, T. L. Long-Cycling Aqueous Organic Redox Flow Battery (AORFB) toward Sustainable and Safe Energy Storage. *J. Am. Chem. Soc.* **2017**, *139*, 1207.
(26) Goulet, M.-A.; Aziz, M. J. Flow Battery Molecular Reactant Stability Determined by Symmetric Cell Cycling Methods. *J. Electrochem. Soc.* **2018**, *165*, A1466.
(27) Milshtein, J. D.; Kaur, A. P.; Casselman, M. D.; Kowalski, J. A.; Modekrutti, S.; Zhang, P. L.; Harsha Attanayake, N.; Elliott, C. F.; Parkin, S. R.; Risko, C.; Brushett, F. R.; Odom, S. A. High Current Density, Long Duration Cycling of Soluble Organic Active Species for Non-Aqueous Redox Flow Batteries. *Energy Environ. Sci.* **2016**, *9*, 3531.
(28) Darling, R. M.; Gallagher, K. G.; Kowalski, J. A.; Ha, S.; Brushett, F. R. Pathways to Low-Cost Electrochemical Energy Storage: A Comparison of Aqueous and Nonaqueous Flow Batteries. *Energy Environ. Sci.* **2014**, *7*, 3459.
(29) Dmello, R.; Milshtein, J. D.; Brushett, F. R.; Smith, K. C. Cost-Driven Materials Selection Criteria for Redox Flow Battery Electrolytes. *J. Power Sources* **2016**, *330*, 261.
(30) Albertus, P.; Manser, J. S.; Litzelman, S. Long-Duration Electricity Storage Applications, Economics, and Technologies. *Joule* **2020**, *4*, 21.
(31) https://www.vanadiumprice.com/ (accessed 2019-12-18).
(32) Crawford, A.; Viswanathan, V.; Stephenson, D.; Wang, W.; Thomsen, E.; Reed, D.; Li, B.; Balducci, P.; Kintner-Meyer, M.; Sprenkle, V. Comparative Analysis for Various Redox Flow Batteries Chemistries Using a Cost Performance Model. *J. Power Sources* **2015**, *293*, 388.
(33) Zheng, M.; Sun, J.; Meinrenken, C. J.; Wang, T. Pathways toward Enhanced Techno-Economic Performance of Flow Battery Systems in Energy System Applications. *Journal of Electrochemical Energy Conversion and Storage* **2019**, *16*, 021001.
(34) *Lazard's Levelized Cost of Storage Analysis*. https://www.lazard.com/media/450774/lazards-levelized-cost-of-storage-version-40-vfinal.pdf (2018).
(35) Kwabi, D. G.; Ji, Y.; Aziz, M. J. Electrolyte Lifetime in Aqueous Organic Redox Flow Batteries: A Critical Review. *Chem. Rev.* **2020**, DOI: 10.1021/acs.chemrev.9b00599.
(36) Goulet, M.-A.; Tong, L.; Pollack, D. A.; Tabor, D. P.; Odom, S. A.; Aspuru-Guzik, A.; Kwan, E. E.; Gordon, R. G.; Aziz, M. J. Extending the Lifetime of Organic Flow Batteries via Redox State Management. *J. Am. Chem. Soc.* **2019**, *141*, 8014.

https://dx.doi.org/10.1021/acsenergylett.0c00140
ACS Energy Lett. 2020, 5, 879−884

Supplementary Information

Lifetime and Cost of Redox-Active Organics for Aqueous Flow Batteries

Fikile R. Brushett [§,*], *Michael J. Aziz*[†,*], *and Kara E. Rodby*[§]

§ Department of Chemical Engineering, Massachusetts Institute of Technology, Cambridge, MA 02139, USA
† John A. Paulson School of Engineering and Applied Sciences, Harvard University, Cambridge, MA 02138, USA
*brushett@mit.edu (Fikile R. Brushett); maziz@harvard.edu (Michael J. Aziz).

Techno-economic Calculations

Capital cost (C_{capital}) is calculated by summing the electrolyte cost ($C_{\text{electrolyte}}$) the net present value of the future costs of electrolyte replacement ($NPV(C_{\text{electrolyte}})$), and the power costs ($C_{\text{power}}$) divided by the duration (d):

$$C_{\text{capital}}\ (\$/\text{kWh}) = C_{\text{electrolyte}} + \frac{C_{\text{power}}}{d} + NPV(C_{\text{electrolyte}}) \quad \textbf{(S1)}$$

$C_{\text{electrolyte}}$ is calculated using a bottom-up approach developed by Dmello *et al.* [1]:

$$C_{\text{electrolyte}}\ (\$/\text{kWh}) = \frac{\left[\frac{c^{+}_{\text{active}} \bullet s^{+} \bullet MW^{+}}{\chi^{+} \bullet n_{e}^{+}} + \frac{c^{-}_{\text{active}} \bullet s^{-} \bullet MW^{-}}{\chi^{-} \bullet n_{e}^{-}} + 2 \bullet r_{\text{avg}} \bullet MW_{\text{salt}} \bullet c_{\text{salt}} + \frac{2}{b_{\text{avg}}} \bullet c_{\text{solvent}}\right]}{F \bullet U \bullet \varepsilon_{\text{sys,d}} \bullet \varepsilon_{\text{v,d}} \bullet \varepsilon_{\text{q,rt}}} \quad \textbf{(S2)}$$

where the names of most variables are listed in **Table S1**. r_{avg} is the mean molar salt ratio (mol/mol), MW_{salt} and c_{salt} are the molecular weight (kg/mol) and cost of the supporting salt ($/kg), respectively, b_{avg} is the mean actives molality (mol/kg), and c_{solvent} is the cost of solvent ($/kg). The + and – superscripts denote the positive and negative electrolyte, respectively.

Here, we assume a symmetric electrolyte, meaning the costs and technical properties are the same for the positive and the negative electrolytes (note: this holds for the vanadium redox flow battery). Additionally, we assume that for aqueous systems the costs of the active species are significantly

more than those of the solvent and salt ($c_{solvent} + c_{salt} << c_{active}$) [1,2]. With these two assumptions, we reduce Equation S2:

$$C_{\text{electrolyte}}\ (\$/\text{kWh}) = \frac{2 \bullet \frac{c_{\text{active}} \bullet s \bullet MW}{\chi \bullet n_e}}{F \bullet U \ \bullet \varepsilon_{\text{sys,d}} \bullet \varepsilon_{\text{v,d}} \bullet \varepsilon_{\text{q,rt}}} \quad \textbf{(S3)}$$

We take the baseline values for the variables in this equation from the Dmello *et al.* paper, as listed in **Table S1** [1].

Table S1 – Variable names, symbols, units, and baseline values for capital calculations (equations S1-S5). Most values are taken from Dmello *et al.* (2016) [1], which followed the work of Darling *et al.* (2014) [2], and correspond to future cost and performance projections. Other parameters were estimated based on the literature and best guesses at future projections.

Variable Name	Symbol	Units	Baseline Value
Open circuit potential	U	V	1
Depth of discharge	χ	-	0.8
Voltage discharge efficiency	$\varepsilon_{v,d}$	%	91.6%
System discharge efficiency	$\varepsilon_{sys,d}$	%	94%
Round-trip coulombic efficiency	$\varepsilon_{q,rt}$	%	97%
Stoichiometric coefficient	s	-	1
Number of electrons per s formula unit	n_e	-	1
Cost of active species	c_{active}	$/kg	12.5
Molecular weight of active species	MW	g/mol	150
Cost per unit area	c_a	$/m^2 of active area	122.5
Balance-of-plant costs	c_{BOP}	$/kW	102.5
Additional costs	c_{add}	$/kW	87.5
Area-specific resistance	ASR	Ω-cm^2	1
Discount rate	r	-	0.08
Operational lifetime	n	years	20
Annual electrolyte replacement fraction	f	-	0.15

C_{power} is calculated using a similar bottom-up approach from Dmello *et al.* [1]:

$$C_{\text{power}}\ (\$/\text{kW}) = \frac{c_{\text{a}} \bullet ASR}{\varepsilon_{\text{sys,d}} \bullet \varepsilon_{\text{v,d}} \bullet (1-\varepsilon_{\text{v,d}}) \bullet U^2} + c_{\text{BOP}} + c_{\text{add}} \quad \textbf{(S4)}$$

where the names of most variables are listed in **Table S1**.

Finally, the net present value of the future costs of electrolyte replacement is calculated using a classic net present value equation:

$$NPV(C_{\text{electrolyte}}) = C_{\text{electrolyte}} \bullet f \bullet \sum_{t=1}^{n-1} \frac{1}{(1+r)^t} = C_{\text{electrolyte}} \bullet f \bullet \frac{(1+r)^{-1} - (1+r)^{-n}}{1-(1+r)^{-1}} \quad \textbf{(S5)}$$

where the definition of $C_{\text{electrolyte}}$ can be found in equations S2 and S3. All analyses in **Figure 5** of the main text use the baseline values in **Table S1** unless specified otherwise.

In **Figure 5**, we further define a new variable called the "total active cost," ($C_{\text{active}}^{\text{total}}$):

$$C_{\text{active}}^{\text{total}} = c_{\text{active}} \bullet \left[1 + f \bullet \frac{(1+r)^{-1} - (1+r)^{-n}}{1-(1+r)^{-1}} \right] \quad \textbf{(S6)}$$

This variable encompasses all of the effects of the cost of active species and its periodic replacement. We can further encapsulate the other important, tunable parameters of organics (i.e., molecular weight and number of electron transfers per mole of active species) that will strongly affect the electrolyte and thus capital costs by transforming the active cost from a weight basis to a charge basis:

$$c_{\text{active}}\ (\$/\text{kAh}) = \frac{c_{\text{active}}\ (\$/\text{kg}) \bullet MW}{F \bullet n_{\text{e}}} \bullet 3.6\ \text{e6}\ (\text{C/kAh}) \quad \textbf{(S7)}$$

Finally, there is a comparison to the capital cost of an all vanadium redox flow battery (VRFB) in **Figure 5a** of the main text. All baseline values for the parameters in **Table S1** were used, except for the open circuit voltage (changed to 1.4 V), the electrolyte replacement fraction (changed to 0, as rebalancing for VRFBs allows essentially infinite electrolyte lifetime), and the active cost on a per charge basis. To calculate the active cost, which corresponds to the green line in **Figure 5a** of the main text, is the average price for Chinese vanadium pentoxide flake (98% purity by weight), calculated from daily price data from the past three years [3]. Daily prices were linearly interpolated in the limited regions where data points were not provided. The shaded green regions represent the +/- standard deviation from the mean (n = 1,093). Values for vanadium pentoxide prices were converted from units of \$/kg into \$/kAh using the following equation:

$$c_{\mathrm{V}}\ (\$/\mathrm{kAh}) = \frac{c_{\mathrm{V_2O_5}}\ (\$/\mathrm{kg}) \bullet MW_{\mathrm{V_2O_5}} (\$/\mathrm{kg\ V_2O_5}) \bullet 3.6\ \mathrm{e6}\ (\mathrm{C/kAh})}{w_{\mathrm{V_2O_5}} \bullet F\ (\mathrm{C/mol\ e^-}) \bullet 2\ (\mathrm{mol\ e^-\ /\ mol\ V_2O_5})} \quad \textbf{(S8)}$$

where c_V is the price per kAh of vanadium, $C_{V_2O_5}$ is the price per kg of vanadium pentoxide (27.22 +/- 14.90 $/kg), $MW_{V_2O_5}$ is the molecular weight of vanadium pentoxide (181.88 e-3 kg/mol), and $w_{V_2O_5}$ is the weight purity of vanadium pentoxide (0.98).

References

[1] R. Dmello, J.D. Milshtein, F.R. Brushett, K.C. Smith, Cost-driven materials selection criteria for redox fl ow battery electrolytes, J. Power Sources. 330 (2016) 261–272. doi:10.1016/j.jpowsour.2016.08.129.

[2] R.M. Darling, K.G. Gallagher, J.A. Kowalski, H. Seungbum, F.R. Brushett, Pathways to low-cost electrochemical energy storage : a comparison of aqueous and nonaqueous flow batteries, (2015) 3459–3477. doi:10.1039/C4EE02158D.

[3] Vanadium Price, (2019). https://www.vanadiumprice.com/ (accessed December 18, 2019).